HHS Public Access

Author manuscript

Clin Neurophysiol. Author manuscript; available in PMC 2022 June 01.

Published in final edited form as:

Clin Neurophysiol. 2021 June ; 132(6): 1321–1329. doi:10.1016/j.clinph.2021.01.027.

Biophysical Characterization of Local Field Potential Recordings from Directional Deep Brain Stimulation Electrodes

M. Sohail Noor, **Cameron C. McIntyre**

Department of Biomedical Engineering, Case Western Reserve University, Cleveland, OH, USA

Abstract

Objective: Two major advances in clinical deep brain stimulation (DBS) technology have been the introduction of local field potential (LFP) recording capabilities, and the deployment of directional DBS electrodes. However, these two technologies are not operationally integrated within current clinical DBS devices. Therefore, we evaluated the theoretical advantages of using directional DBS electrodes for LFP recordings, with a focus on measuring beta-band activity in the subthalamic nucleus (STN).

Methods: We used a computational model of human STN neural activity to simulate LFP recordings. The model consisted of 235,280 anatomically and electrically detailed STN neurons surrounding the DBS electrode, which was previously optimized to mimic beta-band synchrony in the dorsolateral STN. We then used the model system to compare LFP recordings from cylindrical and directional DBS contacts, and evaluate how the selection of different contacts for bipolar recording affected the LFP measurements.

Results: The model predicted two advantages of directional DBS electrodes over cylindrical DBS electrodes for STN LFP recording. First, recording from directional contacts could provide additional insight on the location of a synchronous volume of neurons within the STN. Second, directional contacts could detect a smaller volume of synchronous neurons than cylindrical contacts, which our simulations predicted to be a ~0.5 mm minimum radius.

Conclusions: STN LFP recordings from 8-contact directional DBS electrodes (28 possible bipolar pairs) can provide more information than 4-contact cylindrical DBS electrodes (6 possible bipolar pairs), but they also introduce additional complexity in analyzing the signals.

Significance: Integration of directional electrodes with DBS systems that are capable of LFP recordings could improve opportunities to localize targeted volumes of synchronous neurons in PD patients.

Corresponding Author: Cameron C. McIntyre, Ph.D., Department of Biomedical Engineering, Case Western Reserve University, 2103 Cornell Road, Rm 6224, Cleveland, OH 44106, USA, ccm4@case.edu.

Conflict of Interest Statement

CCM is a paid consultant for Boston Scientific Neuromodulation, receives royalties from Hologram Consultants, Neuros Medical, Qr8 Health, and is a shareholder in the following companies: Hologram Consultants, Surgical Information Sciences, CereGate, Autonomic Technologies, Cardionomic, Enspire DBS.

Keywords

Parkinson's Disease; Subthalamic Nucleus; Neuron; Synchrony; Oscillation; Beta

1. Introduction

Subthalamic deep brain stimulation (DBS) is an established treatment for the symptoms of advanced Parkinson's disease (PD). DBS therapy has provided extensive opportunities to record local field potentials (LFPs) from the subthalamic nucleus (STN), which have subsequently expanded understanding of the pathophysiology of PD [Oswal et al., 2013]. Major conclusions from those experimental LFP studies have been the identification of STN beta-band (12–30 Hz) synchrony as a correlate of PD symptoms [e.g. Kuhn et al., 2009], and that the concepts of LFP-based adaptive DBS appear promising for advancing DBS therapy [Meidahl et al., 2017]. Along those lines, recent advances in clinical DBS devices [Stanslaski et al., 2018] are facilitating the opportunity to use chronic LFP recordings in control systems that modulate the delivery of stimulation for the treatment of PD [Velisar et al., 2019]. However, the currently available adaptive DBS prototype systems employ traditional cylindrical electrode contacts, which are thought to limit LFP recording specificity [Zhang et al., 2018].

Directional electrodes represent another important advance in the clinical armamentarium of DBS technology [Steigerwald et al., 2019]. Several clinical studies have established the utility of being able to direct stimulation to different sides of the DBS electrode in attempts to avoid capsular side effects [e.g. Contarino et al., 2014; Dembek et al, 2017]. In addition, directional DBS electrodes have been used to acutely measure LFP signals in PD patients, demonstrating that STN beta-band activity can be preferentially recorded on different sides of the electrode [e.g. Bour et al., 2015, Tinkhauser et al., 2018]. Unfortunately, commercially available directional DBS electrodes are not currently compatible with clinical implanted pulse generators that enable chronic LFP recording. Nonetheless, integration of these two core technologies would appear to have synergistic benefits.

The goal of this study was to explore the biophysics of STN LFP recording with directional DBS electrodes, and then evaluate how different bipolar recording configurations affect the LFP measurements. The use of bipolar contact pairs on the DBS lead is the preferred method for clinical LFP recording [Marmor et al. 2017]. However, it is currently unclear how to best select the bipolar recording contacts on a directional DBS lead to either maximize signal amplitude or interpret the relative location of a synchronous volume of neurons to those contacts. Therein lies the value of a detailed model system that is parameterized to mimic the human STN in a PD state. Maling et al. [2018] created a DBS LFP model that was optimized to simulate beta-band synchrony in the dorsolateral STN, based on chronic clinical LFP recordings from a PD patient [Quinn et al., 2015]. That LFP model system was originally developed with a 4-contact cylindrical DBS lead, but in this study we replaced it with an 8-contact directional DBS lead. As such, we created a computational tool that facilitated direct comparison of the LFP recordings from cylindrical vs. directional contacts, with cellular-level detail in a clinically relevant context.

2. Methods

This study analyzed simulated LFP recordings from DBS electrodes implanted in the STN using a computational model (Figures 1, 2). The technical details of the model system are described in their entirety in Maling et al. [2018], and briefly expanded upon below. The patient imaging data used to construct the model was from a 52 year old male with tremor-dominate PD [Quinn et al., 2015]. The model was constructed for the right side of the brain. The STN was represented with model neurons that provided the electrical sources for the LFP simulations. These electrical sources were integrated with a finite element volume conductor electric field model that included the DBS lead. The volume conductor model was designed to be representative of recording from either the Medtronic 3389 lead or the Boston Scientific 2202 lead. We then recorded the voltages at the DBS electrode contacts, which resulted from all of the time-varying current sources generated by the STN neuron models [Lempka and McIntyre, 2013].

2.1. Subthalamic Nucleus Model

The Maling et al. [2018] STN LFP model system defined anatomical volumes that represented the subcortical structures of interest within the patient-specific magnetic resonance image (MRI) (Figure 1A). The focus of that process was the definition of a STN volume and the localization of the DBS lead within the patient anatomy. The STN volume was populated with 235,280 multi-compartment neuron models, providing a neuron density consistent with human histological measurements of STN neurons [Levesque and Parent, 2005] (Figures 1B, 2A). The neuron models were used to simulate the transmembrane currents that provide the electrical sources for the LFP signals (Figures 2B, 2C) [Maling et al., 2018].

The geometry of the STN neuron models was based on 3D anatomical reconstructions of macaque STN neurons [Sato et al., 2000]. The electrical properties of the neuron models were parameterized to mimic experimentally defined transmembrane currents and action potential firing characteristics of STN neurons [Gillies and Willshaw, 2006; Miocinovic et al., 2006]. Each STN neuron model also received 290 different synaptic input currents distributed over its structure [Lempka and McIntyre, 2013]. These synaptic currents were intended generically represent the thousands of synapses and hundreds of pre-synaptic axons that contribute to the neural activity of the STN neuron. Each synaptic input was activated for each synaptic input timing trigger assigned to each specific neuron (see additional details below). The somatic and dendritic compartments of each neuron model received either an excitatory or inhibitory synaptic input, with the inhibitory currents being slightly delayed [Baufreton et al., 2005]. While not explicitly modeled as such, the excitatory and inhibitory synaptic inputs could be loosely considered to represent hyperdirect and pallidal input streams to the STN neurons.

Each of the STN neuron models received unique time varying synaptic inputs [Maling et al., 2018]. The STN neurons were designated to receive either a synchronous beta pattern of synaptic inputs, or asynchronous synaptic inputs (Figure 2B). For the beta synchronous population of neurons, synaptic inputs were generated every 50 ms (i.e. 20 Hz) with temporal jitter that was randomly chosen from a normal distribution with a standard

deviation of 6.25 ms. For the asynchronous population, each neuron received synaptic inputs at a rate randomly taken from an exponential distribution with a mean and standard deviation of 50 ms (i.e. 20 Hz). Neurons in the beta synchronous pool exhibited highly correlated activity, while the neurons in the asynchronous pool exhibited uncorrelated activity [Maling et al., 2018]. For the LFP simulations, the net current flowing across the membrane of each compartment (365) of each neuron (235,280) was represented as an independent time-varying current source (85,877,200 total sources).

2.2 Volume Conductor Model

The volume conductor model of the brain tissue medium and DBS electrode was represented as a finite element model (FEM) [Lempka and McIntyre, 2013]. Each DBS electrode contact in the FEM was modeled as a highly conductive piece of metal with the size and shape of the clinical electrode contact. The DBS electrode was surrounded by a 0.1 mm interface layer, mimicking tissue encapsulation, and that was surrounded by the bulk brain tissue. We assigned the bulk brain tissue a conductivity of 0.2 S/m, and the interface layer a conductivity of 0.03 S/m [Maling et al., 2018]. For the 3389 DBS lead model, the electrode impedance of cylindrical contact 2 was 913 Ω. For the 2202 DBS lead model, the electrode impedance of contact 1 was 877 Ω, directional contact 5 was 2780 Ω, and contact 8 was 909 Ω. The volume conductor model was created in COMSOL v5.4 (Burlington, MA). The default electrode position used in this study was defined from the patient-specific imaging data of the subject analyzed in Maling et al. [2018] (Figure 1).

To simulate STN LFP recordings, we coupled the volume conductor model and electrical source models using a reciprocity-based solution [Lempka and McIntyre, 2013]. In the coupled FEM-neuron population model, each compartment of each neuron was represented as an independent current source at the appropriate spatial location in the FEM. The LFP recording at a DBS contact was then calculated by summing the voltages imposed upon that contact from all of the transmembrane currents [Maling et al., 2018] (Figure 2C). Differential recordings for any bipolar pair of contacts could then be defined by subtracting the time series voltage signal recorded at one contact from the time series voltage signal recorded at the other contact.

2.3. Optimized STN LFP Model

To optimize the STN LFP model to the patient, Maling et al. [2018] considered the shape of the power spectrum and the distribution of power in the beta-band across the electrode array using a fitness metric that included two components. The first component was the Pearson's correlation coefficient between the model power spectra and the clinical power spectrum at each of the simultaneously recorded bipolar contact pairs. The second component was the asymmetry ratio that compared the relative normalized beta-band power at each contact pair. Three bipolar pairs of simultaneous clinical LFP recordings from the patient, acquired with a 4-contact cylindrical 3389 DBS lead and Activa PC+S, were used in combination with an optimization algorithm to customize the neural activity parameters in the STN LFP model to best match the patient data [Maling et al., 2018] (Figure 2C). The optimized model predicted a 2.4 mm radius volume of 36,580 beta synchronous neurons located in the dorsolateral STN (Figure 2B).

2.4. Directional DBS Electrode Model

The main goal of this study was to apply the optimized Maling et al. [2018] STN LFP model (Figure 2) to the theoretical analysis of recordings from directional DBS electrodes (Figure 3). We compared the simulated recordings from the 4-contact cylindrical DBS lead with an 8-contact directional DBS lead. All aspects of the STN LFP model system were held constant, aside from replacing the Medtronic 3389 lead with a Boston Scientific 2202 lead. The 8-contact directional DBS lead was positioned such that the 5-6-7 ring of contacts exactly corresponded to contact 2 of the 4-contact cylindrical DBS lead (Figure 1A). The directional marker, and contacts 2–5, pointed anterior in the patient anatomy.

We used the model system to explore three questions: 1) How does the amplitude of the LFP signal change when recording from different directional contacts? 2) How does the selection of different bipolar contact pairs affect the recorded LFP signal? and 3) What is the smallest volume of beta synchronous STN neurons that can be robustly detected with LFP recordings from DBS electrodes? To address the first two questions, we used the STN neural activity patterns defined by the optimized Maling et al. [2018] STN LFP model (Figure 2). To address the third question, we used spherical populations (radii of 1.00, 0.50, or 0.25 mm) of beta synchronous neurons within the STN volume.

3. Results

The main advantage of using an anatomically and electrically detailed STN LFP model to evaluate recording with cylindrical versus directional DBS contacts is the opportunity to position the different electrode designs in identical locations within the neuroanatomy and compare their recordings from identical time-varying electrical sources. As such, the differences noted in the time series LFP recordings are explicitly related to the differences in electrode design. Figure 3 provides example simulations of the most simple and direct comparison between cylindrical and directional recordings. Contact 2 of the 3389 lead and contacts 5-6-7 of the 2202 lead exactly correspond to each other with respect to their position in the STN. Monopolar recording (i.e. a very distant reference electrode) at contact 2 of the 3389 lead generates a peak-to-peak signal amplitude that is less than the signal recorded at contact 5 of the 2202 lead (which points toward the synchronous STN neurons), but greater than contact 7 of the 2202 lead (which points away from the synchronous STN neurons). As such, the directionality of the recordings from the 2202 lead is generated by the relative position of the specific contact to the synchronous volume of STN neurons (Figure 3). Similarly, averaged recording from contacts 5-6-7 of the 2202 lead generates a LFP signal that is identical to contact 2 of the 3389 lead (Supplemental Material, Figure S1).

Monopolar recordings are conceptually useful for comparison purposes, but clinical recordings typically use bipolar configurations (i.e. the reference electrode contact is also on the DBS lead) because they help to cancel common mode noise and eliminate volume-conducted signals from distant brain regions [Marmor et al. 2017]. Lempka and McIntyre [2013] and Maling et al. [2018] provided detailed biophysical analyses of bipolar recordings from the 3389 lead, and clinical decisions on the selection of bipolar pairs for the 3389 lead are relatively straightforward. However, 8-contact directional leads have 28 possible bipolar pairs for recording. In addition, LFP recording from directional leads also introduces

questions on using not only close versus distant contacts for bipolar recording, but also large versus small contacts, and rotational (i.e. on the same cylindrical level) versus vertical (i.e. on different cylindrical levels) contacts.

Figure 4 provides examples of the LFP signal, simulated from identical STN neural activity, for a range of bipolar recording options that use contact 5 of the 2202 lead. Not surprisingly, we found that the recording configuration had an effect on the amplitude of the LFP signal. For example, referencing contact 5 with respect to contact 1 produced a signal that most closely corresponded to the monopolar LFP (one contact inside the beta synchronous volume and the other contact completely outside the beta synchronous volume). Referencing contact 5 with respect to contact 2 resulted in the lowest signal amplitude (both contacts within the beta synchronous volume). An alternative variant of Figure 4 is provided in the Supplemental Material (Figure S2) with information on the power spectral density of the simulated LFPs.

The simulated LFP signals (Figure S3) and spectrograms (Figure S4) from each of the 28 bipolar recording configurations of the directional lead are provided in the Supplemental Material. A useful note from those simulation is that simple assumptions, such as close versus distant bipolar configurations are thought to generate higher versus lower LFP signal amplitudes, are actually context dependent (Supplemental Material, Figure S5). The specifics of the LFP signal recorded from a given bipolar pair are dictated by the location and size of the synchronous volume of neurons relative to the individual electrode contacts [Lempka and McIntyre, 2013; Maling et al., 2018] (Supplemental Material, Figure S3).

The location of the DBS electrode in the STN also affects the LFP signal. Figure 5 provides direct comparison between LFP simulations recorded at the default location (Location 1 - posterior STN), and two alternate locations. Location 2 and 3 placed contact 5 in the center and anterior STN respectively. As expected, bipolar LFP signal with contact 5 varies substantially as the electrode position is changed. The amplitude is larger when one of the two contacts (used in the bipolar configuration) is close to the synchronous volume and smaller when either both contacts are near or far from the synchronous population.

Given the substantial clinical interest and technical focus on beta-band activity in STN LFP studies, it would be useful to know the smallest population of beta synchronous STN neurons that can generate a detectable beta-band oscillation on DBS electrodes. Therefore, we used our STN LFP model system to compare LFP recordings generated by small volumes of beta synchronous neurons with either the 4-contact cylindrical DBS lead or the 8-contact directional DBS lead (Figure 6). The recorded LFP signal was filtered with techniques representative the control signal used in recent adaptive STN DBS clinical studies [Little et al. 2016]. We positioned a small volume of synchronous STN neurons very close to contact 2 of the 2202 lead (or contact 1 of the 3389 lead), and computed the bipolar LFP with reference to contact 1 (or contact 0 of the 3389 lead). We then modulated the size of that synchronous volume (radius = 0.25; 0.50; 1.00 mm) and monitored the filtered beta-band signal. The amplitude of the LFP recording, signal-to-noise ratio (SNR), and filtered beta-band signal, all decreased as the radius of the synchronous neuron population decreased (Figure 6). For the 2202 lead, we estimate that a threshold radius to observe beta-band

oscillations in the filtered signal was approximately 0.5 mm. For the 3389 lead, the results suggest that a larger radius of synchronous neurons would be necessary to reliably detect beta-band oscillations. However, it should be noted that these approximations are for synchronous volumes of neurons that are very close to the electrode (centered ~1 mm away). As such, the results in Figure 6 represent a “best case” scenario for detecting small volume oscillations. If, for example, the small volume was further away (centered ~2 mm from the DBS electrode) the 2202 and 3389 leads would both need an ~1 mm radius of synchronous neurons to be able to detect the beta-band signal (Supplemental Material, Figure S6).

The minimum detectable volume analysis only represents a thought experiment. The actual spatial distribution of synaptic inputs and neural synchronization patterns exhibited by small volumes of STN neurons are not know at the level of physiological detail that would be needed to accurately address the minimum detectable volume question in vivo. However, the results presented in Figure 6 do highlight the fact that a directional contact orientated toward a region of neural synchrony does exhibit a higher SNR than a cylindrical contact. This occurs because the smaller surface area of the directional contact results in a higher input impedance, and the LFP recording voltage imposed upon the contact is not averaged across the larger surface area of the cylindrical contact. A directional contact oriented away from the synchronous volume exhibits a lower SNR than the cylindrical contact, primarily because it is geometrically farther away from the sources (Figure 3).

4. Discussion

Clinical recordings of LFPs from DBS electrodes implanted in the STN have provided key insights into the pathophysiology of PD. One finding of special interest has been the correlative association between PD symptoms and excessive beta-band activity [Oswal et al., 2013], especially long-duration bursts of beta-band activity [Deffains et al., 2018]. As such, the concept of using beta-band activity as a control signal for DBS modulation has been extensively investigated [Cagnan et al., 2019], and the first examples of real-world clinical utility are becoming available [Velisar et al., 2019]. However, while it is clear that beta-band LFP signals can be used to successfully modulate DBS therapy, there remain several engineering questions on the optimization of things like the signal processing steps, control system strategy, and recording electrode design. Many of these engineering questions can be initially addressed using appropriately parameterized computer models to help guide the next iteration of clinical experiments. With that goal in mind, this study used a detailed STN LFP model system to better characterize the role of electrode design and bipolar recording configuration on the biophysical interpretation of LFP recordings.

A logical next step in the technical evolution of adaptive DBS therapy for PD is to use directional electrodes to improve the density and specificity of the LFP recordings [Zhang et al., 2018]. This next step would expand the number of possible bipolar recording pairs from 6 with the 3389 Medtronic lead, to 28 with the commercially available directional leads (2202 Boston Scientific lead, or 6172 Abbott lead). In addition, the directional lead designs provide LFP signal amplitude information that is modulated by the orientation of the directional contacts relative to the synchronous population of neurons (Figures 3, 4, 5) [Bour et al., 2015, Tinkhauser et al., 2018]. Therefore, directional lead designs theoretically enable

the collection of more information than cylindrical lead designs, and this additional information should be useful in defining the size and location of synchronous volumes of neurons that surround the DBS lead.

One interesting caveat that needs to be considered when performing clinical LFP experiments with the current commercially available directional leads is the mismatch in contact impedance for bipolar recording between contacts with different surface areas (e.g. contact 5 and 1 of the 2202 lead (Figures 4, 5)). The simulated LFP signals presented in this study represent theoretically idealized results generated by differential recordings at the contacts. However, because of the mismatch in contact impedance between large and small recording contacts, a common mode signal will be present in the bipolar recordings. Experimental LFP recordings must be fed through an amplifier, and if there is a mismatch in the impedance of the contacts, there can be issues associated with the rejection of common mode signals, especially stimulus artifacts. Therefore, investigators need to be aware of these issues when using different sized contacts for bipolar LFP recording and account for them in their recording setup.

A key assumption in the design of typical LFP-based adaptive DBS strategies is that the synchronous volume of neurons generating the biomarker signal is also a target of the stimulation for therapeutic benefit. If that assumption is true, then the most detailed characterization possible for that target volume would be useful in stimulation parameter selection [Yoshida et al. 2010; Ince et al., 2010]. While we have shown that a reasonable estimate of the synchronous volume can be defined in the STN from just 3 simultaneous bipolar LFP recordings [Maling et al., 2018], the computational advantages of using 28 bipolar pairs in predictive models are substantial from both robustness and accuracy perspectives. In addition, the clinical utility of controlling the stimulation volume with directional electrodes provides greater opportunities to subsequently focus stimulation on that target volume [Steigerwald et al., 2019]. Therefore, directional electrode designs theoretically provide advantages, over traditional cylindrical electrode designs, for both stimulation and recording applications in bidirectional DBS systems.

While there may be technical benefits associated with using directional DBS leads, the expanded complexity of analyzing and interpreting LFP signals from an 8-contact directional electrode are also important issues to consider. Even the most savvy STN LFP experts would find difficulty in mentally integrating 28 different signals streaming off the lead (Supplemental Material, Figures S3, S4), and then developing an estimate of the size and location of beta-band synchrony in the STN (Figures 3, 4, 5). As such, a transition to 8-contact directional lead designs in bidirectional DBS systems is likely to require more elaborate processing within the implanted pulse generator, as well as a clinician/researcher software interface that is capable of providing more detailed analysis of the signals. Therefore, we propose that source localization computational models could provide useful tools within that kind of software [Thompson et al., 2018]. Those models could conceivably be as detailed and complex as the patient-specific STN LFP simulations used in the study. However, it is much more likely that simple representations of time-varying point sources surrounding the DBS lead will provide a more tractable modeling option. Either way, a coupled source and electrode model, integrated with an optimization algorithm, could be

used to provide an estimate on the size and location of a beta-band synchrony volume (or other processed signal) for a given time window of LFP recordings [Maling et al., 2018]. That model-based information could then be used to help guide the electrode contact selection processes for both stimulation and recording in the patient.

The main goal of this study was to provide a direct comparison of simulated STN LFP recordings from cylindrical and directional DBS electrode contacts. The model system we used to perform that comparison is the most technically advanced and anatomically detailed model of STN LFPs ever assembled. However, that model system still suffers from numerous limitations that are explained in Maling et al. [2018]. Some of those limitations include using a simple volume conductor model that hinders simulation of the 1/f distribution in the power spectrum, and a macaque STN neuron model (which are smaller than human STN neurons) that likely reduces the amplitude of the LFP simulations. As such, the simulated LFP amplitudes in the model [Maling et al., 2018] were less than the clinical recordings acquired with the Activa PC+S in the original patient [Quinn et al., 2015]. However, the ~30 μV peak-to-peak beta-band recordings generated by the model are consistent with subthalamic LFP recordings from DBS electrodes using experimental recording rigs with known amplifier and filter settings [e.g. Brown and Williams, 2005].

The STN LFP model limitation that is most relevant to this study is likely to be the representation of synaptic inputs to the STN neuron models. First, the model system condensed the thousands of pre-synaptic inputs onto each STN neuron into generic representations of a few hundred inhibitory and excitatory currents [Lempka and McIntyre, 2013]. These synaptic currents were tuned to generate activity patterns in the STN neurons that correspond with experimental recordings, but the true magnitude and temporal characteristics of the synaptic currents are unknown. Second, we relied on the simplifying assumption of using a single spherical volume of beta synchronous STN neurons to represent the optimized patient-specific LFP simulation. Maling et al. [2018] made that assumption as a basic first step for the development of conceptual guidelines in the biophysical interpretation of clinical STN LFP signals. The patient-specific STN LFP model infrastructure actually allows for the use of any synaptic input pattern to any of the neurons, and is capable of simulating much more complicated forms of neural synchrony. However, creating a realistically constrained model that coincides with the limited number of clinical recording channels (3 in the original study), presents a situation where attempting to optimize more than a single synchronous volume would just be an exercise in model overfitting. Therein lies an additional motivation to use directional DBS electrodes in STN LFP studies. The simultaneous acquisition of 28 channels of LFP data would greatly expand the detail and specificity of simulated beta synchronous volumes that could be realistically represented in a patient-specific LFP model. Those results could then be helpful in addressing more detailed questions on the anatomical localization of beta-band activity in the STN, and the consistency (or lack thereof) of those localizations over time in the same PD patient, and/or across populations of PD patients.

5. Conclusion

Clinical LFP measurements with directional DBS contacts in the STN have shown that beta-band signal amplitudes can differ across the directional recordings. This study augmented those clinical observations using models with explicit knowledge of the electrode position within the anatomy, as well as the region of beta-band neural synchrony, all relative to the individual DBS recording contacts. As such, the model allows for the demonstration of general concepts that are relevant to the acquisition of clinical LFP recordings, and highlights the additional complexity associated with analyzing LFP signals from directional DBS contacts.

Supplementary Material

Refer to Web version on PubMed Central for supplementary material.

Acknowledgements

This work was supported by a grant from the National Institutes of Health (R01 MH106173; R01 NS119520). The authors also thank Nicholas Maling and Angela Noecker for assistance with the model development.

References

Baufreton J, Atherton JF, Surmeier DJ, Bevan MD. Enhancement of excitatory synaptic integration by GABAergic inhibition in the subthalamic nucleus. J Neurosci. 25(37):8505–8517, 2005. [PubMed: 16162932]

Bour LJ, Lourens MA, Verhagen R, de Bie RM, van den Munckhof P, Schuurman PR, Contarino MF. Directional Recording of Subthalamic Spectral Power Densities in Parkinson's Disease and the Effect of Steering Deep Brain Stimulation. Brain Stimul. 8(4):730–741, 2015. [PubMed: 25753176]

Brown P, Williams D. Basal ganglia local field potential activity: character and functional significance in the human. Clin Neurophysiol. 116(11):2510–9, 2005. [PubMed: 16029963]

Cagnan H, Denison T, McIntyre C, Brown P. Emerging technologies for improved deep brain stimulation. Nat Biotechnol. 37(9):1024–1033, 2019. [PubMed: 31477926]

Contarino MF, Bour LJ, Verhagen R, Lourens MA, de Bie RM, van den Munckhof P, Schuurman PR. Directional steering: A novel approach to deep brain stimulation. Neurology. 83(13):1163–9, 2014. [PubMed: 25150285]

Deffains M, Iskhakova L, Katabi S, Israel Z, Bergman H. Longer β oscillatory episodes reliably identify pathological subthalamic activity in Parkinsonism. Mov Disord. 33(10):1609–1618, 2018. [PubMed: 30145811]

Dembek TA, Reker P, Visser-Vandewalle V, Wirths J, Treuer H, Klehr M, Roediger J, Dafsari HS, Barbe MT, Timmermann L. Directional DBS increases side-effect thresholds-A prospective, double-blind trial. Mov Disord. 32(10):1380–1388, 2017. [PubMed: 28843009]

Gillies A, Willshaw D. Membrane channel interactions underlying rat subthalamic projection neuron rhythmic and bursting activity. J Neurophysiol. 95(4):2352–2365, 2006. [PubMed: 16148272]

Ince NF, Gupte A, Wichmann T, Ashe J, Henry T, Bebler M, Eberly L, Abosch A. Selection of optimal programming contacts based on local field potential recordings from subthalamic nucleus in patients with Parkinson's disease. Neurosurgery. 67(2):390–7, 2010. [PubMed: 20644424]

Kühn AA, Tsui A, Aziz T, Ray N, Brücke C, Kupsch A, Schneider G-H, Brown P. Pathological synchronisation in the subthalamic nucleus of patients with Parkinson's disease relates to both bradykinesia and rigidity. Exp Neurol. 215(2):380–387, 2009. [PubMed: 19070616]

Lempka SF, McIntyre CC. Theoretical analysis of the local field potential in deep brain stimulation applications. PLoS One. 8(3):e59839, 2013.

Levesque JC, Parent A. GABAergic interneurons in human subthalamic nucleus. Mov Disord. 20(5):574–584, 2005. [PubMed: 15645534]

Little S, Beudel M, Zrinzo L, Foltynie T, Limousin P, Hariz M, Neal S, Cheeran B, Cagnan H, Gratwicke J, Aziz TZ, Pogosyan A, Brown P. Bilateral adaptive deep brain stimulation is effective in Parkinson's disease. J Neurol Neurosurg Psychiatry. 87(7):717–721, 2016. [PubMed: 26424898]

Maling N, Lempka SF, Blumenfeld Z, Bronte-Stewart H, McIntyre CC. Biophysical basis of subthalamic local field potentials recorded from deep brain stimulation electrodes. J Neurophysiol. 120(4):1932–1944, 2018. [PubMed: 30020838]

Marmor O, Valsky D, Joshua M, Bick AS, Arkadir D, Tamir I, Bergman H, Israel Z, Eitan R. Local vs. volume conductance activity of field potentials in the human subthalamic nucleus. J Neurophysiol. 117(6):2140–2151, 2017. [PubMed: 28202569]

Meidahl AC, Tinkhauser G, Herz DM, Cagnan H, Debarros J, Brown P. Adaptive Deep Brain Stimulation for Movement Disorders: The Long Road to Clinical Therapy. Mov Disord. 32(6):810–819, 2017. [PubMed: 28597557]

Miocinovic S, Parent M, Butson CR, Hahn PJ, Russo GS, Vitek JL, McIntyre CC. Computational analysis of subthalamic nucleus and lenticular fasciculus activation during therapeutic deep brain stimulation. J Neurophysiol. 96(3):1569–1580, 2006. [PubMed: 16738214]

Oswal A, Brown P, Litvak V. Synchronized neural oscillations and the pathophysiology of Parkinson's disease. Curr Opin Neurol. 26(6):662–670, 2013. [PubMed: 24150222]

Quinn EJ, Blumenfeld Z, Velisar A, Koop MM, Shreve LA, Trager MH, Hill BC, Kilbane C, Henderson JM, Bronte-Stewart H. Beta oscillations in freely moving Parkinson's subjects are attenuated during deep brain stimulation. Mov Disord. 30(13):1750–1758, 2015. [PubMed: 26360123]

Sato F, Parent M, Levesque M, Parent A. Axonal branching pattern of neurons of the subthalamic nucleus in primates. J Comp Neurol. 424(1):142–152, 2000. [PubMed: 10888744]

Stanslaski S, Herron J, Chouinard T, Bourget D, Isaacson B, Kremen V, Opri E, Drew W, Brinkmann BH, Gunduz A, Adamski T, Worrell GA, Denison T. A Chronically Implantable Neural Coprocessor for Investigating the Treatment of Neurological Disorders. IEEE Trans Biomed Circuits Syst. 12(6):1230–1245, 2018. [PubMed: 30418885]

Steigerwald F, Matthies C, Volkmann J. Directional Deep Brain Stimulation. Neurotherapeutics. 16(1):100–104, 2019. [PubMed: 30232718]

Thompson JA, Oukal S, Bergman H, Ojemann S, Hebb AO, Hanrahan S, Israel Z, Abosch A. Semi-automated application for estimating subthalamic nucleus boundaries and optimal target selection for deep brain stimulation implantation surgery. J Neurosurg. May 18:1–10, 2018. doi: 10.3171/2017.12.JNS171964.

Tinkhauser G, Pogosyan A, Debove I, Nowacki A, Shah SA, Seidel K, Tan H, Brittain JS, Petermann K, di Biase L, Oertel M, Pollo C, Brown P, Schuepbach M. Directional local field potentials: A tool to optimize deep brain stimulation. Mov Disord. 33(1):159–164, 2018. [PubMed: 29150884]

Velisar A, Syrkin-Nikolau J, Blumenfeld Z, Trager MH, Afzal MF, Prabhakar V, Bronte-Stewart H. Dual threshold neural closed loop deep brain stimulation in Parkinson disease patients. Brain Stimul. 12(4):868–876, 2019. [PubMed: 30833216]

Yoshida F, Martinez-Torres I, Pogosyan A, Holl E, Petersen E, Chen CC, Foltynie T, Limousin P, Zrinzo LU, Hariz MI, Brown P. Value of subthalamic nucleus local field potentials recordings in predicting stimulation parameters for deep brain stimulation in Parkinson's disease. J Neurol Neurosurg Psychiatry. 81(8):885–9, 2010. [PubMed: 20466699]

Zhang S, Connolly AT, Madden LR, Vitek JL, Johnson MD. High-resolution local field potentials measured with deep brain stimulation arrays. J Neural Eng. 15(4):046019, 2018.

HIGHLIGHTS

- Detailed model of human subthalamic nucleus local field potential (LFP) recordings with deep brain stimulation electrodes.
- Compared LFP signals recorded with cylindrical vs. directional contacts.
- Directional contacts can enable higher signal-to-noise ratio recordings than cylindrical contacts.

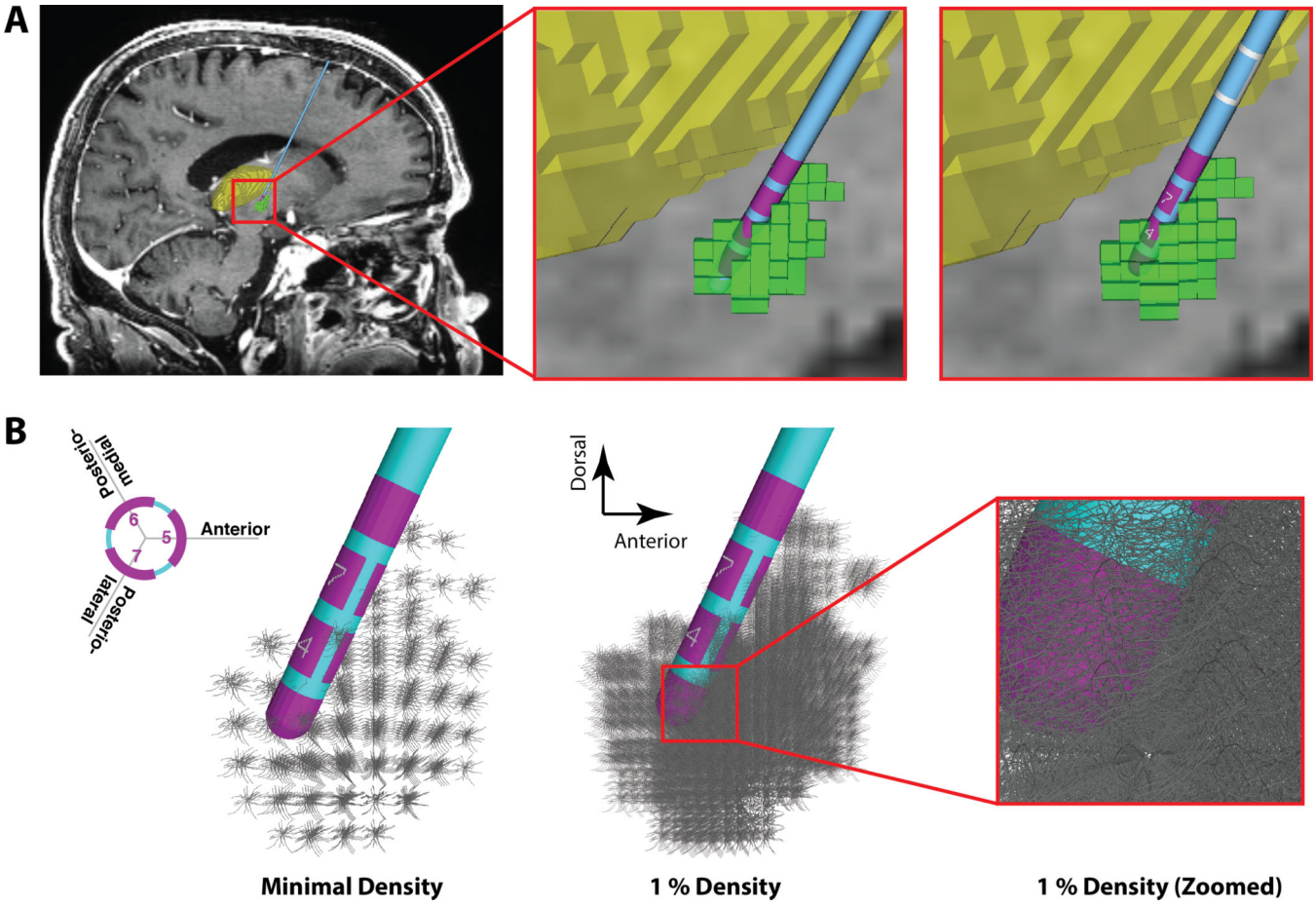

Figure 1.

Anatomical Model. A) Far left panel shows a sagittal view of the patient magnetic resonance image (MRI), deep brain stimulation (DBS) electrode, and 3D anatomical volumes representing the subthalamic nucleus (STN - green) and thalamus (yellow). Middle panel shows a zoomed-in view of the original patient-specific 3389 lead location (pink electrode contacts). Far right panel shows the corresponding 2202 lead location. B) STN neuron models surrounding the DBS electrode. Each grey STN neuron model is displayed with its full 3D geometry of the soma-dendritic architecture. Far left panel, one model neuron is shown in each voxel of the STN volume (185 neurons). Middle panel, 1% density of the STN neurons models (i.e. 2350 out of 235,280 neurons), and right-most panel displays a zoomed-in view around contact 1.

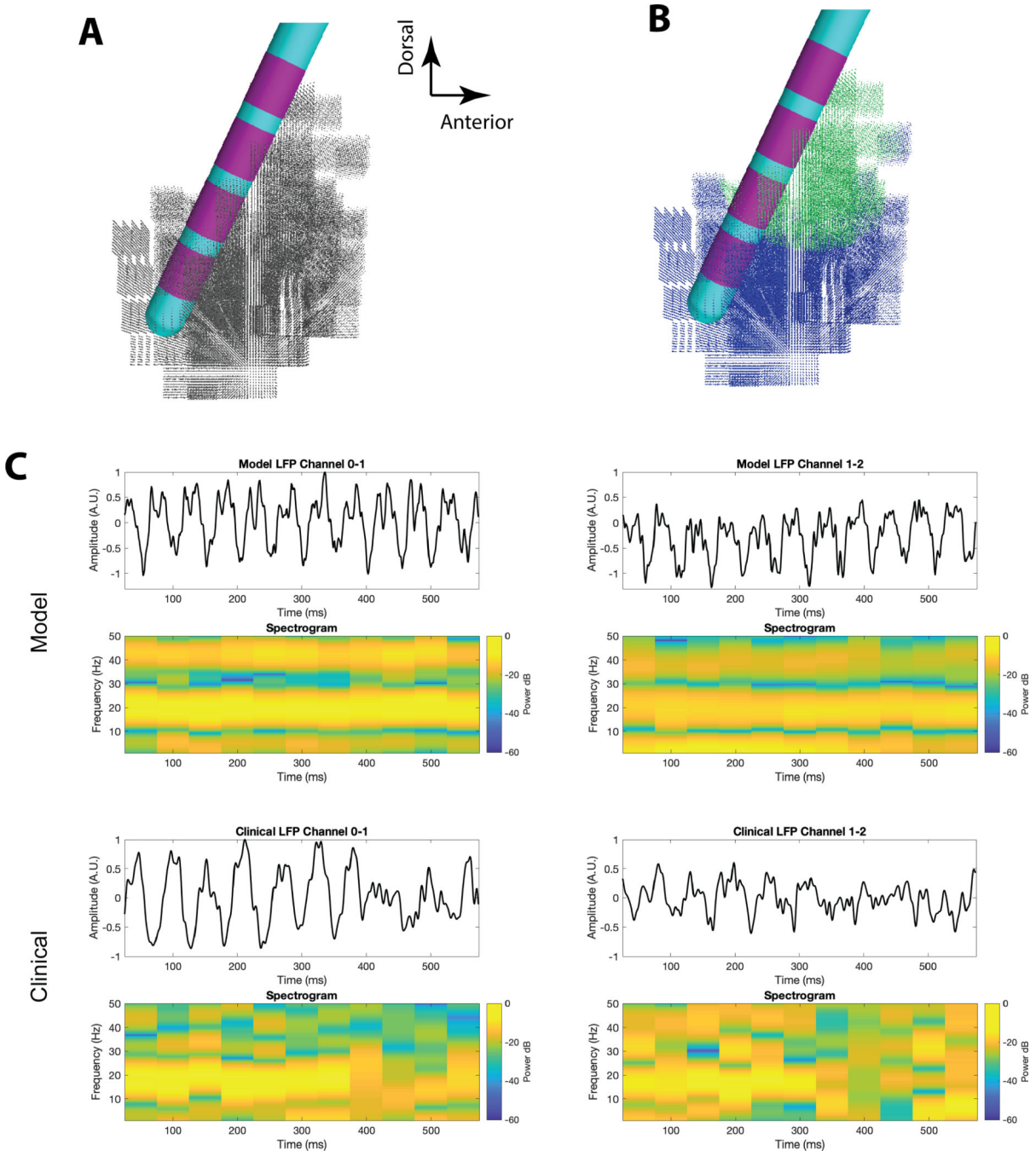

Figure 2.

Subthalamic Local Field Potential (LFP) Model. A) Pictorial representation of the 3389 lead within the subthalamic nucleus (STN) model. The location of each cell body of each of the 235,280 STN neuron models is identified by a grey dot. B) Pictorial representation of the optimized Maling et al. [2018] STN LFP model. Beta-synchronous STN neurons are identified by green dots. Asynchronous STN neurons are identified by blue dots. C) Example comparisons of the clinical LFP signal with the simulated LFP generated by the optimized model. Adapted from Maling et al. [2018].

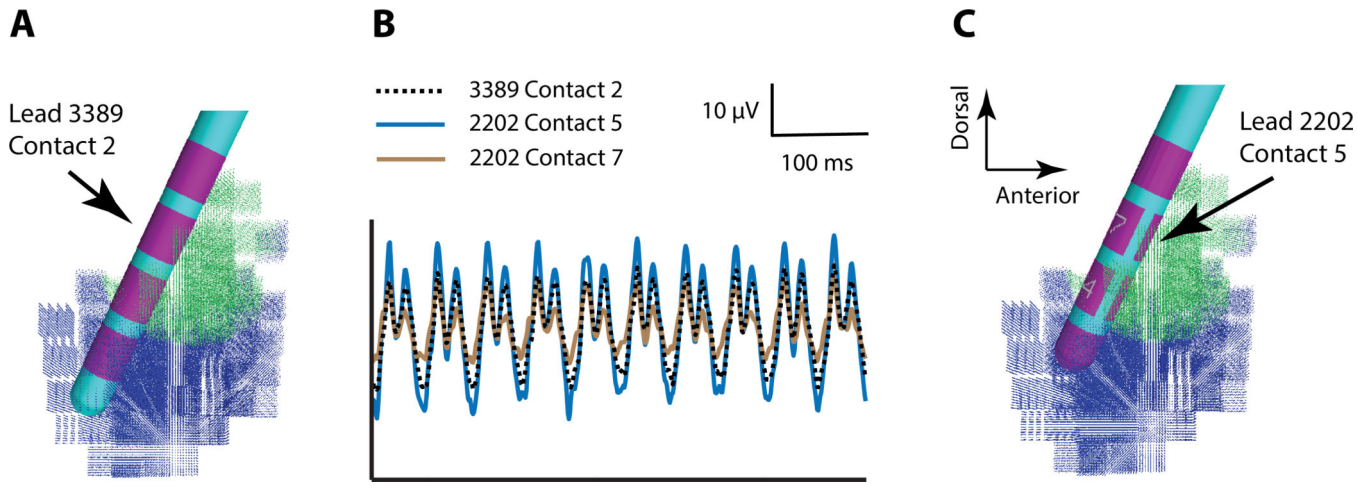

Figure 3.

Monopolar Recordings. A) 3389 lead in the subthalamic local field potential (LFP) model. B) Example simulated monopolar recordings from specific deep brain stimulation (DBS) electrode contacts. C) 2202 lead in the subthalamic LFP model.

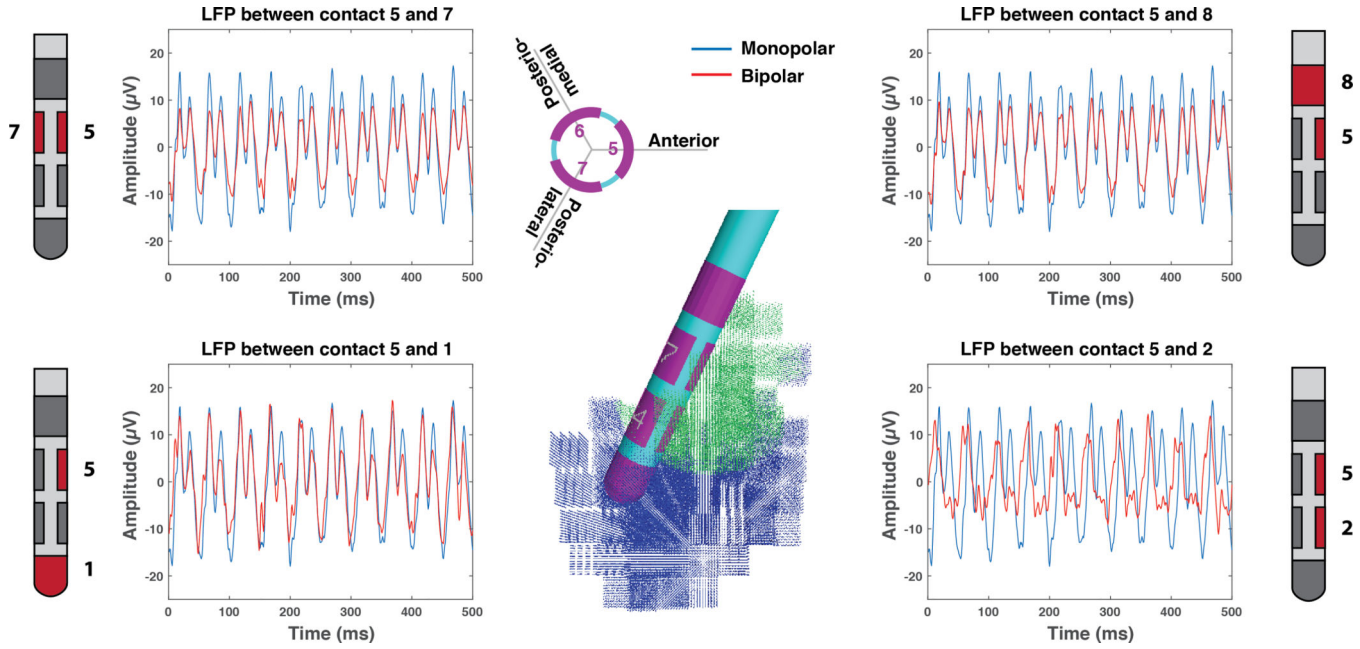

Figure 4.

Directional Recordings. Example simulated local field potential (LFP) recordings with contact 5 of the 2202 lead. The monopolar LFP for contact 5 is provided for reference with each bipolar LFP example.

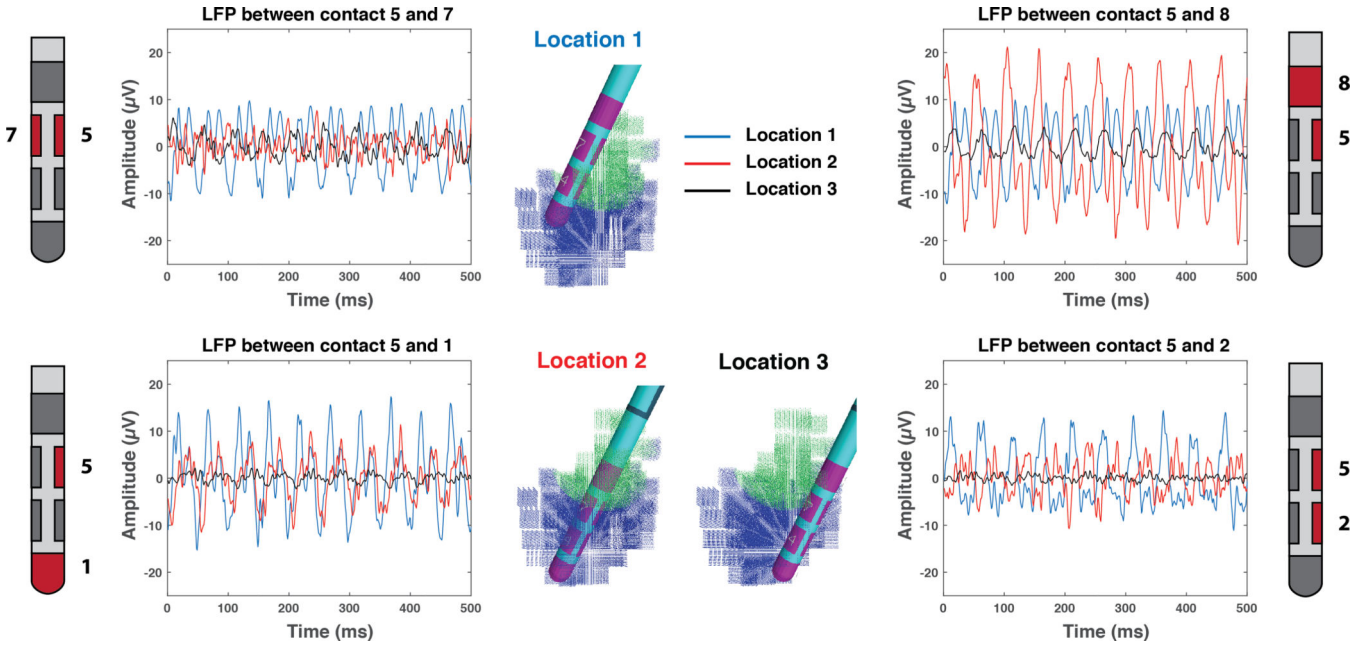

Figure 5.

Electrode Location. Example simulated local field potential (LFP) recordings with contact 5 of the 2202 lead. The deep brain stimulation (DBS) electrode is placed in 3 different locations relative to the subthalamic nucleus (STN). Location 1 is the default position used in all other figures. Location 2 has contact 5 placed in the center of the STN. Location 3 has contact 5 placed in the anterior STN.

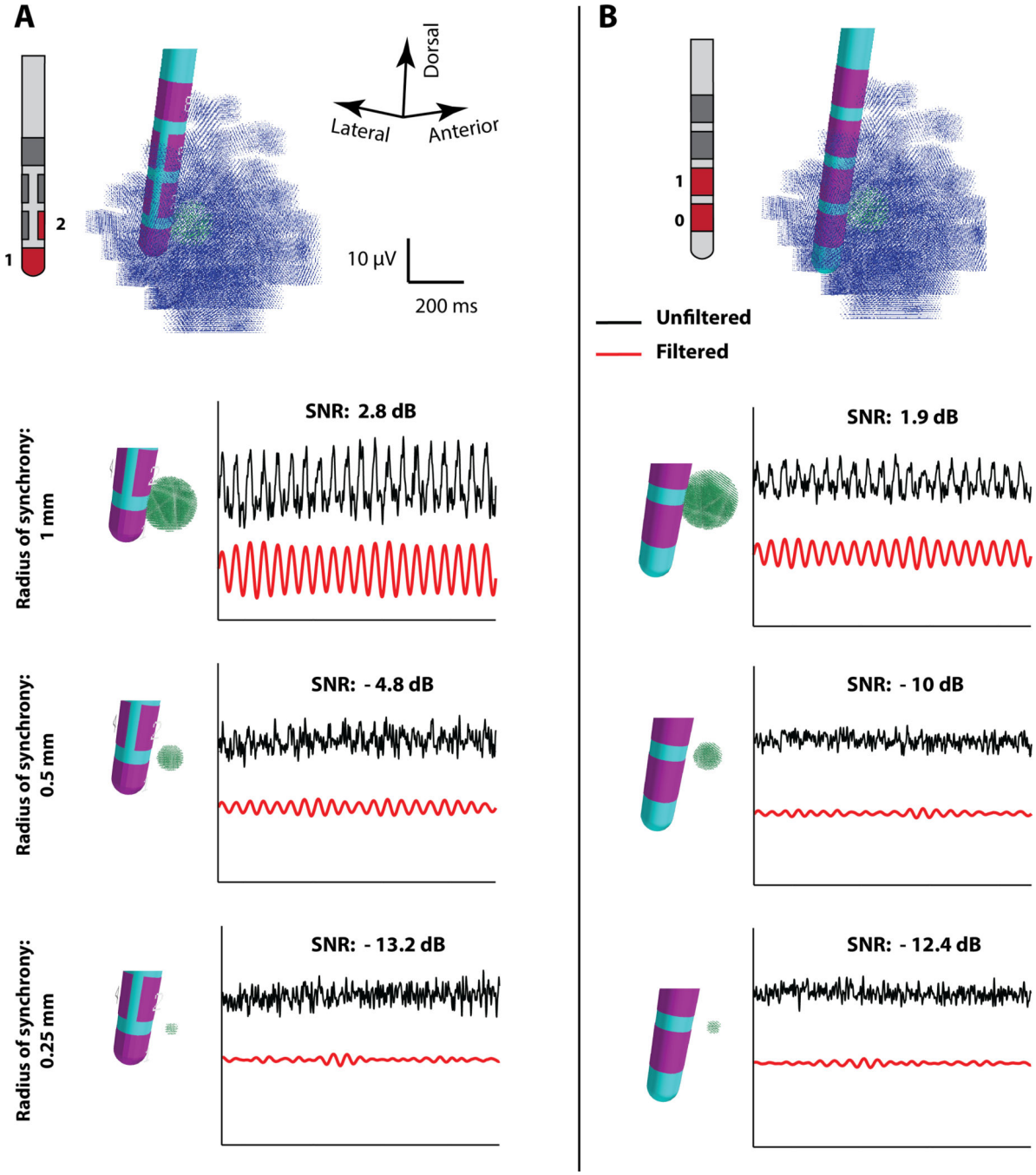

Figure 6.

Minimal Detectable Volume. Side-by-side comparison of the filtered and unfiltered local field potential (LFP) signals simulated with the (A) 2202 lead and (B) 3389 lead, from small beta synchronous volumes of 1.00, 0.50, and 0.25 mm radii, located 1 mm from the lead. The LFP was filtered with a bandpass filter (4-pole, Butterworth) with cut-off frequencies of 17 and 23 Hz to create a simulated beta-band control signal. An oblique view of the subthalamic LFP model is shown at the top of each column, with the synchronous and asynchronous neuron models displayed as green dots or blue dots, respectively. Bipolar

recordings and signal-to-noise ratio (SNR) are presented for the 1–2 pair of the 2202 lead (A), or the 0–1 pair of the 3389 lead (B).